Comprehensive transcriptomic analysis shows disturbed calcium homeostasis and deregulation of T lymphocyte apoptosis in inclusion body myositis

Mridul Johari[1,2]*, MSc, Anna Vihola[1,2,3], PhD, Johanna Palmio[4], MD, PhD, Manu Jokela[3,5], MD, PhD, Per Harald Jonson[1,2], PhD, Jaakko Sarparanta[1,2], PhD, Sanna Huovinen[6], MD, Marco Savarese[1,2], PhD, Peter Hackman[1,2], PhD, Bjarne Udd[1,2,4,7], MD, PhD

[1]Folkhälsan Research Center, Helsinki, Finland
[2]Department of Medical Genetics, Medicum, University of Helsinki, Finland
[3]Neuromuscular Research Center, Department of Genetics, Fimlab Laboratories, Tampere, Finland
[4]Neuromuscular Research Center, Department of Neurology, Tampere University and University Hospital, Tampere, Finland
[5]Division of Clinical Neurosciences, Department of Neurology, Turku University Hospital, Turku, Finland
[6]Department of Pathology, Fimlab Laboratories, Tampere University Hospital, Tampere, Finland
[7]Department of Neurology, Vaasa Central Hospital, Vaasa, Finland

*Corresponding Author
Mridul Johari, MSc
Folkhälsan Research Center,
Department of Medical Genetics, Medicum, University of Helsinki
Biomedicum, Haartmaninkatu 8, PO Box 63, FI-00014 Helsinki, Finland
Email: mridul.johari@helsinki.fi
Tel (office): +358 2941 25629

Abstract

Objective: Inclusion body myositis (IBM) has an unclear molecular etiology due to the co-existence of characteristic cytotoxic T-cell activity and degeneration of muscle fibers. Using in-depth gene expression and splicing studies, we aimed at understanding the different components of the molecular pathomechanisms in IBM.

Methods: We performed RNA-seq on total RNA extracted from skeletal muscle biopsies of clinically and histopathologically defined IBM (n=24), tibial muscular dystrophy (n=6), and histopathologically normal controls (n=9). In a comprehensive transcriptomics analysis, we analyzed the differential gene expression, differential splicing and exon usage, downstream pathway analysis, and the interplay between coding and non-coding RNAs (micro RNAs and long non-coding RNAs).

Results: We observe IBM-specific dysregulation of genes involved in calcium homeostasis, particularly affecting the T-cell activity and regulation, causing disturbed Ca^{2+} induced apoptotic pathway of T cells in IBM muscles. Additionally, LCK/p56, which is an essential gene in regulating the fate of T-cell apoptosis, shows altered expression and splicing usage in IBM muscles

Interpretation: Our analysis provides a novel understanding of the molecular mechanisms in IBM by showing a detailed dysregulation of genes involved in calcium homeostasis and its effect on T-cell functioning in IBM muscles. Loss of T-cell regulation is hypothesized to be involved in the consistent observation of no response to immune therapies in IBM patients. Our results show that loss of apoptotic control of cytotoxic T cells in IBM could indeed be one component of their abnormal cytolytic activity in IBM muscles.

Introduction

Inclusion body myositis (IBM) is a late-onset, acquired muscle disease with unclear etiology, and the poorly understood molecular pathogenesis is under debate due to several factors. The CD8+ T-cell infiltration and overexpression of class I MHC antigens in all muscle fibers indicate an autoimmune cascade and are, in fact, the most consistent finding together with the degeneration of myofibers. However, IBM largely remains refractory to immunosuppressive drugs[1], and comprehensive clinical trials have generally been ineffective[2]. A partial clinical and histopathological overlap with other rimmed-vacuolar (RV) myopathies[3], the occurrence of rare familial cases[4], and the protein accumulations in the RVs[5] support a degenerative muscle pathology. Additionally, previous studies showing a strong genetic association with 8.1 ancestral haplotype[6, 7] support a possible genetic predisposition for IBM. Accumulation/aggregation of these misfolded proteins suggests that IBM could be a protein aggregate disease with immune-mediated cytotoxic inflammation as a resulting secondary feature[8]. However, there is a significant variance in nature and the number of accumulated proteins observed in the IBM muscle biopsies[9]. Similar aggregates observed in HIV-associated IBM[10] suggest that protein aggregation can still be a downstream effect of immune dysfunction.

Analysis of tissue-specific mRNAs and subsequent RNA-seq based transcriptomics studies focused on understanding the expression of genes, participating pathways, and networks can increase our understanding of underlying pathomechanisms. Prior studies have investigated the differential gene expression in IBM muscles for both the inflammatory and the degenerative pathology[11-17]. However, no study has attempted a comprehensive analysis of RNA-seq data combining differential gene expression, differential exon, and splicing usage along with in-depth analysis of the relation between dysregulation of coding and regulatory RNAs in IBM muscles.

Our study used total RNA extracted from muscle biopsies of IBM patients, of non-myositis RV-myopathy disease controls, and non-muscle disease controls. We first studied the differential expression of coding, long non-coding RNAs (lncRNAs), and micro RNAs (miRNAs) and then evaluated their possible interplay. Additionally, we studied the transcriptome-wide differential exon and splicing usage. We observed a significant association with genes involved in various calcium-related pathways and identified disturbed calcium regulation specific to T cells in IBM muscles, highlighting the relevance of calcium homeostasis for T-cell activity in IBM muscles. In particular, we identified calcium-induced T lymphocyte apoptosis to be disturbed in IBM muscles.

Materials and methods

Patients and skeletal muscle biopsies

Muscle biopsies (predominantly Tibialis anterior or Vastus lateralis) from 24 Finnish patients diagnosed with clinically and pathologically defined IBM according to the ENMC criteria[18] were included. The age of onset was 60 ± 11 years (median ± SD), and the age at muscle biopsy was 70 ± 9 years. Additionally, muscle biopsies from six patients with genetically diagnosed Tibial muscular dystrophy (TMD, caused by heterozygous FINmaj mutation the titin gene)[19] were included. In the TMD cohort, the age of onset was 49 ± 11 years, and age at biopsy 54 ± 14 years. Nine muscle biopsies from individuals that underwent leg amputation for reasons other than a muscle disease[20] were also included. These nine biopsies did not show pathologically defined muscle degeneration or inflammation. Age at sampling for amputees was 70 ± 11 years. All muscle biopsies were snap-frozen and stored at -80 °C. Muscle biopsies were collected at the Tampere Neuromuscular Research Center, Tampere University Hospital, Finland.

Ethical approval for this study falls under HUS:195/13/03/00/11. Informed consent from the patients was obtained at the time of sample collection.

RNA extraction, selection, and library preparation

Muscle tissue homogenization steps were performed using SpeedMill PLUS (Analytik Jena AG, Germany). RNA was extracted with Qiagen RNeasy Plus Universal Mini Kit (Qiagen, Hilden, Germany) according to the manufacturer's instructions. According to the manufacturer's guidelines, extracted RNA was treated with Invitrogen TURBO DNAse buffer (ThermoFisher Scientific, MA, USA). RNA was quantified and qualitatively assessed using High Sensitivity RNA ScreenTape (Agilent Technologies, CA, USA) on Agilent 4200 TapeStation system (Agilent Technologies).

Library preparations and sequencing were performed at Oxford Genomics Center, University of Oxford. For PolyA+ RNA selection, the NEBNext Ultra II Directional RNA Library Prep kit (E7760) for Illumina (NEB, Beverly, MA, USA) was used to prepare strand-specific RNA-seq libraries. Libraries were multiplexed and sequenced on HiSeq4000: 75bp paired-end sequencing (Illumina, CA, USA), and an average of ~47 million reads per sample were produced. Samples with enough RNA were used for library preparation for small RNA (< 200 nt) selection (18 IBM, nine amputees, and four TMD). NEBNext Small RNA Library Prep Set (E7330) for Illumina was used per the manufacturer's instructions (NEB). Libraries were multiplexed and sequenced on HiSeq2500: 50bp single-end sequencing (Illumina), and an average of ~10 million reads per sample were produced.

112 RNA-seq data pre-processing, QC, and alignment

113 Adapter sequences and low-quality bases were removed with fastp[21]. Trimmed sequences were then
114 mapped with STAR 2.7.0d[22] (STAR, RRID: SCR_004463) with index generated from Gencode.v29
115 human reference (release date 05.2018, based on ENSEMBL GRCh38.p12) and comprehensive gene
116 annotation (primary assembly) using the STAR two-pass method according to the guidelines from
117 the ENCODE project for alignment of long RNA (>200 nt) and small RNA (<200 nt) data.

118 RNA-seq quantification and differential gene expression analysis

119 Uniquely mapped fragments were summarized and quantified (referred to as counts) by
120 featureCounts[23] (featureCounts, RRID: SCR_012919) using Gencode.v29 primary comprehensive
121 gene annotation which lists 58,780 RNAs including 19,969 protein-coding, 16,066 non-coding and
122 22,745 other types of RNAs (primary gene expression analysis). Separate quantification of counts for
123 lncRNA (lncRNA analysis) was done using long non-coding RNA gene annotation from
124 Gencode.v29 (a subset of the primary annotation). Quantification of counts for miRNAs (miRNA
125 analysis) in 31 samples was done using miRBase human miRNA annotation (Release 22.1 October
126 2018)[24]. DGE analysis was performed with DESeq2[25] (v1.26.0) (DESeq2, RRID: SCR_015687) in
127 Rstudio (v1.2.5019) (RStudio, RRID: SCR_000432) based on R (v3.6.3) (R Project for Statistical
128 Computing, RRID: SCR_001905). Counts were normalized with variance stabilizing transformation
129 function within DESeq2. A principal component analysis (PCA) was performed on the gene
130 expression data of the IBM samples compared to amputee and TMD controls. Further, pairwise
131 comparisons between cohorts were performed using the Wald test. Log_2 fold changes (LFC) were
132 shrunk using 'ashr' adaptive shrinkage estimation[26], and results were generated with default
133 independent filtering for increasing power. Only genes with LFC values larger than ±1.5 and a
134 Benjamini-Hochberg adjusted p-value of ≤0.01 were considered further. Genes specifically
135 dysregulated in IBM muscles were considered for downstream analysis.

136 Pathway analysis

137 Ingenuity Pathway Analysis (IPA, QIAGEN Inc.) (Ingenuity Pathway Analysis, RRID:
138 SCR_008653) was used for pathway analysis and enrichment analysis of the obtained DGE data.
139 Using Ingenuity Pathways Knowledge Base (Ingenuity Pathways Knowledge Base, RRID:
140 SCR_008117), IPA mapped and annotated genes to the pathways and predicted activation state based
141 on the direction of changes comparing it with the change in the database.

142

143 Differential splicing analysis

144 To investigate differential usage of exons and splicing, independent of the differential gene
145 expression analysis, we used QoRTS[27] java-based application (v1.3.6) (QoRTs, RRID: SCR_018665)
146 to prepare counts from exons and splice junctions (known and novel) from the aligned data.
147 Downstream analysis of this data was performed using JunctionSeq[28] (v1.16.0) in R. JunctionSeq
148 results produce a q-value (based on FDR) on gene-level analysis, which considers that one or more
149 exon/junction in this gene is differentially used. A conservative q-value threshold of 0.01 was used
150 to select significant observations. IBM-specific differentially expressed genes, and differentially
151 spliced genes were compared (Fig 1). Statistical over-enrichment analysis for Gene ontology terms
152 in categories: Molecular function, biological process, and cellular component, was performed on
153 results obtained from QoRTs/JunctionSeq using clusterProfiler[29] (clusterProfiler, RRID:
154 SCR_016884). Gene sets were compared using UpSet plot[30].

155 Data availability

156 Raw counts and normalized DESeq2 counts from polyA+ RNAs and miRNAs are available in GEO
157 as superseries GSE151758.

158 Results

159 Expression signature is significantly different in IBM muscles as compared to control muscles

160 Fig 1a shows the summarized workflow of the methodology. The PCA shown in Fig 1b explains the
161 differences between the three cohorts. Pairwise comparisons were performed to reduce the potential
162 confounding effects of controls, which identified 2,288 and 302 genes specifically up- or down-
163 regulated in the IBM cohort, respectively (Fig 1c). Non-coding RNA analyses resulted in 497
164 lncRNAs upregulated, 106 lncRNAs downregulated, 140 miRNAs upregulated, and 126 miRNAs
165 explicitly downregulated in the IBM cohort compared to control groups. These IBM-specific
166 dysregulated RNAs were used for downstream pathway analysis using IPA workflow. The top 15
167 genes dysregulated specifically in IBM muscles, with their functional annotations and normalized
168 expression in the different cohorts, are shown in Fig 2.

169 Pathway analysis

170 We performed IPA workflow analysis on IBM-specific dysregulated genes to better understand the
171 pathways and the upstream regulators associated with the observed expression dysregulation. Out of
172 these, 2,588 genes, 596 lncRNAs, and 257 miRNAs mapped to the Ingenuity database. From the

173 primary gene expression analysis, IPA identified 91 pathways as significantly altered. Fig 3a shows
174 a summary of the IPA results with the top identified pathways.

175 The top upstream regulators in both lncRNA analysis and miRNA analysis are shown in Fig 3c and
176 3d, respectively. We identified an increased expression of the lncRNA *DNM3OS* (DNM3 antisense
177 RNA) and *MIAT* (Myocardial infarction associated transcript) from these analyses. IPA suggested
178 this dysregulation may be due to *JDP2* (Jun Dimerization Protein 2) and *TARDBP* (TAR DNA
179 Binding Protein), acting as an upstream regulator of *DNM3OS* and *MIAT* respectively (Fig 3c).

180 Dysregulation of calcium-related pathways in IBM muscles

181 IPA identified calcium-induced T lymphocyte apoptosis as one of the most significant pathways
182 dysregulated in IBM muscles (Fig 3a). Our IBM-specific dataset contained 69 genes with significant
183 dysregulation out of the 232 genes annotated in this pathway. A part of this pathway, including the
184 major players, is shown in Fig 4. Another pathway outside the top results identified that 29 genes
185 (29/208, p = 7.05E-03) significantly dysregulated in our dataset are also involved in calcium
186 signaling. These results prompted us to investigate further for calcium related issues in cellular
187 signaling, and we found that IPA also detects dysregulation of the following processes, mobilization
188 of Ca^{2+} (80 genes), the release of Ca^{2+} (33 genes), quantity of Ca^{2+} (51 genes) and flux of Ca^{2+} (51
189 genes), as significantly disturbed in IBM muscles (Fig 3b).

190 Altered exon usage and splicing pattern in IBM muscles

191 To explore IBM-specific exon usage, we performed an independent transcriptome-wide differential
192 splicing analysis in our three cohorts. We obtained a list of 1,271 differentially spliced genes in IBM
193 from our differential splicing analysis. These transcripts either showed IBM-specific increased usage
194 of a known junction or a known exon or contained a novel exon-exon junction resulting in an
195 alternative isoform. To understand the diverse portfolio of mature mRNAs created from pre-mRNAs,
196 we used gene ontology over-enrichment analysis on these 1,271 differentially spliced genes and
197 identified the first splicing signature specific to IBM muscles. To understand the different classes
198 over-represented in these genes, we performed statistical over-enrichment analysis using
199 clusterProfiler for all three GO categories as seen in Fig. 5 a,b,c. Our analysis showed an enrichment
200 of genes involved in the structure and organization of actin filaments assembly in IBM muscles and,
201 interestingly, proteins involved in mRNA processing and metabolism.

202 We then compared the list of differentially spliced genes with differentially expressed genes in our
203 analysis and found an overlap of 79 genes (Fig. 1d). Next, we wanted to observe the overlap between

204 six different sets of genes, namely IBM specific differentially spliced genes, calcium-induced T
205 Lymphocyte apoptosis, Mobilization of Ca2+, Flux of Ca2+, Quantity of Ca2+, and Release of Ca2+
206 (Fig. 5d). We observed 10 genes to be associated with calcium-related processes; *HLA-DPA1*, *HLA-*
207 *DPB1,* and *HLA-DQB1* are associated with calcium-induced T Lymphocyte apoptosis, *ANXA1* is
208 associated with mobilization, flux, and release of Ca^{2+}, *CCL4* is associated with mobilization, flux,
209 and quantity of Ca^{2+}, *GRK3* and *RARRES2* are associated with mobilization, *SH3KBP1* with flux, and
210 *ITGAM* with the quantity of Ca^{2+}. In particular, one specific differentially spliced gene, *LCK,* is part
211 of all six sets.

212 Fig 6a shows the gene expression of *LCK* in three cohorts, with expression in IBM muscles being
213 significantly higher than the others (log_2FC = +2.86, padj=3.50E-11, ranking = 355/2590).
214 Additionally, Fig 6b shows the differential splicing pattern observed in *LCK* in all three groups. The
215 highlighted E016 corresponds to an alternative exon (chr1:32274818-32274992, GRCh38).

216 Discussion

217 In this study, we aimed to identify a more detailed IBM-specific molecular signature, using different
218 RNA-seq based methods that can help us explore the inflammatory and degenerative parts in depth.
219 Antigen-driven T-cell cytotoxicity is the most reproducible and plausible part of the complex
220 molecular pathomechanism in IBM. However, it remains unknown what antigen drives this IBM-
221 specific immune cascade.

222 As part of the RV pathology, accumulated proteins or the unfolded protein response have been
223 hypothesized to prompt an immune reaction[8]. A recent unbiased proteomics study dissected these
224 RVs in IBM[31]. Interestingly, the protein encoded by one of our top differentially expressed genes,
225 *MYL4,* is also detected in the RVs in IBM along with *ANXA1,* which is both differentially expressed
226 and differentially spliced in IBM muscles. In our study design, we considered TMD, another RV
227 muscle disease but without immune involvement, as a control to understand if there are any RV-
228 specific antigens in IBM muscles. Additionally, using age matched histopathologically normal
229 muscles from amputees, we aimed to understand if general inflammatory signatures can be replicated
230 and studied in more detail using additional methods such as non-coding RNAs and differential
231 splicing studies. Consequently, our strong study design and robust methodology helped us replicate
232 findings from previous studies[11-17] and identify essentially new calcium-related issues in IBM
233 muscles and their link with the altered T-cell cytotoxicity in IBM muscle fibers.

234 We found that several genes contributing to calcium homeostasis are differentially expressed in IBM
235 muscles resulting in dysregulation of several critical pathways, specifically, calcium-induced T

236 lymphocyte apoptosis and related Nur77 signaling. Ca^{2+} is a universal second messenger in T cells,
237 and it is known to regulate proliferation and differentiation of T cells and T-cell effector functions[32].
238 The complexity and duration of Ca^{2+} signals and resultant cytoskeletal rearrangements determine the
239 fate of T cells in response to an antigen[33]. On one hand, a short-term increase in intracellular Ca^{2+}
240 concentration results in the cytolytic activity of T cells; on the other hand, prolonged elevation results
241 in proliferation, differentiation, and maturation of näive T cells into Th1, Th2, and Th17 subtypes and
242 the production of cytokines[32].

243 Ca^{2+} signaling is known to optimize the interaction between T cells and antigen-presenting cells[33].
244 The binding of antigen/MHC complexes ($CD8^+$-MHC class I/$CD4^+$-MHC class II) to T-cell receptors
245 (TCR) activates Src-family protein tyrosine kinases, e.g., LCK and FYN at the cytoplasmic side of
246 the TCR/CD3 complex. Additionally, activation of ZAP-70, a tyrosine kinase associate protein,
247 results in the phosphorylation and activation of the intracellular enzyme phospholipase C-γ1 (PLC-
248 γ1)[32, 33]. PLC-γ1 hydrolyses phosphatidylinositol 4,5-biphosphate (PIP2) to produce two other second
249 messengers, inositol 1,4,5-triphosphate (IP3) and diacylglycerol (DAG). IP3 binds to its receptor
250 (IP3R) on the endoplasmic reticulum (ER) membrane to promote rapid release of Ca^{2+} from ER to
251 the cytosol[32]. However, this release of Ca^{2+} is insufficient for antigen-derived T-cell fate but results
252 in depletion of intracellular Ca^{2+} triggering a rapid influx of Ca^{2+} through activation and opening of
253 Ca^{2+} release-Ca^{2+} activated channels (CRAC) on the plasma membrane formed by different
254 STIM1/ORAI1 combinations[34]. The duration of Ca^{2+} influx is vital for activating the calcineurin-
255 dependent nuclear factor activate T cells (NFAT) transcription pathway[32]. In the cytoplasm,
256 calcineurin removes excess phosphate residues from the N terminus of NFAT, promoting its entry
257 into the nucleus. Disruptions in NFAT signaling can cause several phenotypes, including
258 cardiovascular, musculoskeletal, and immunological diseases[35]. Meanwhile, DAG, another
259 secondary messenger, activates protein kinase C (PKC), which in turn activates the nuclear factor
260 kappa B (NFκB). The duration and complexity of Ca^{2+} signals drive the NFAT/NFκB signaling and
261 determine downstream T-cell activation.

262 The genes in the NR4A family (NR4A1/Nur77, NR4A2/Nurr1, NR4A3/Nor1) act as critical
263 molecular switches in cell survival and inflammation. Human *NR4A1* encodes for a homolog of a
264 mouse protein called Nur77, a zinc transcription factor expressed as an early gene in T cells upon
265 antigen-TCR interaction. In addition to being a transcriptional activator, Nur77 has an apoptotic role
266 in T regulatory fate[36] and other non-genomic proapoptotic functions via mitochondrial interactions
267 with Bcl-2[37]. T cells deficient in Nur77 have been shown to have high proliferation, enhanced T-cell
268 activation, and increased susceptibility for T-cell-mediated inflammatory diseases[38]. The expression

269 of Nur77 is Ca^{2+} dependent and is controlled by the myocyte enhancer factor 2 (MEF2) transcription
270 factor[39], whose DNA-binding and transcriptional activity is enhanced by Calcineurin. Another
271 calcium-dependent transcription factor, CABIN1, acts as a transcriptional repressor of MEF2, thus
272 keeping the Nur77 promoter silent in the absence of a TCR signal[40]. The interaction between CABIN1
273 and calcineurin is influenced by intracellular Ca^{2+} and PKC activation, resulting in
274 hyperphosphorylation of CABIN1 and its subsequent transcription repressing activity. An increase in
275 intracellular Ca^{2+} concentration activates the interaction of the calmodulin family of genes (CALM)
276 with CABIN1, triggering the dissociation of MEF2 from Cabin and MEF2 to become
277 transcriptionally active[41]. In the nucleus, NFAT interacts with MEF2 and enhances its transcriptional
278 activity by recruiting the co-activator p300 for the transcription of Nur77.

279 In our dataset, 69 genes mapping to the calcium-induced T Lymphocyte apoptosis and 72 genes
280 mapping the Nur77 signaling in T Lymphocytes are differentially expressed in IBM muscles. As seen
281 in Figure 4, several essential genes like *ZAP70*, *LCK*, different subunits of Protein Kinase C, and
282 *ATP2A1* which encodes for SERCA, are significantly changed in IBM muscles. Additionally, we also
283 observed genes associated with mobilization of Ca^{2+}, release of Ca^{2+}, quantity of Ca^{2+} and flux of
284 Ca^{2+} as significantly dysregulated in IBM muscles, indicating a possible widespread disturbance with
285 the handling of calcium entry and release in cells. In T cells, especially, this disturbance could
286 dramatically impact their activation, differentiation, and most likely, the regulation of T-cell apoptosis
287 will be disturbed.

288 Apoptosis in T cells is necessary to resolve their inflammatory activity, and defective or delayed
289 apoptosis may contribute to the pathogenesis of inflammatory diseases[42]. In this scenario, loss of
290 apoptotic control could be one mechanism explaining the lack of immune-suppressive therapeutic
291 effect in IBM.

292 The diversity of the skeletal muscle proteome is, among others, dependent on the diversity of exon
293 usage in pre-mRNAs[43]. From our transcriptome-wide splicing analysis within the differentially
294 expressed genes, we identified 79 genes, out of which ten are associated with different calcium-
295 related functions. Amongst these, LCK is a T lymphocyte-specific protein tyrosine kinase involved
296 in downstream events of antigen–TCR interaction. LCK/p56 is essential in transducing signals
297 leading to apoptotic cell death in mature T cells[44], and its activity is tightly regulated to protect against
298 hyperactivation of T cells and autoimmunity, thus maintaining T-cell homeostasis[45]. Moreover, LCK
299 also selectively influences the flux and release of calcium in cells[46]. In our analysis, LCK is both
300 differentially expressed and differentially spliced in IBM muscles. Disturbed T-cell apoptosis and the

301 dysregulation of LCK in IBM muscles provide novel insights into the molecular mechanisms of IBM.
302 Considering the crucial regulatory activity of LCK, it might be a potential therapeutic target for IBM
303 patients.

304 We also observe dysregulation of several non-coding RNAs in our study. Previously, Hamann and
305 colleagues have discussed lncRNAs in the context of IBM[13]. The benefits of our study design,
306 especially the homogenous molecular pathology and the larger sample size, let us dig deeper into the
307 dysregulation of lncRNAs specific to IBM muscles. We identified specific JDP2 (DNA binding
308 transcription factor) and TARDBP/TDP-43 (DNA and RNA binding protein), may have altered
309 regulator activity since their downstream non-coding partners (*DNM3OS* and *MIAT,* respectively) are
310 significantly overexpressed IBM muscles. Additionally, both these proteins are specific to RNA
311 polymerase II (RNA Pol II), facilitating transcription and pre-mRNA maturation. Alteration in RNA
312 or DNA binding proteins (expression or localization) associated with the activity of the spliceosome
313 machinery can directly affect the downstream events. Since TDP-43 is accumulated in RVs, one
314 possibility is that the unavailability of TDP-43 can affect its transcription and splicing activities. The
315 normal expression of *TARDBP* we observe in IBM patients is expected and is in coherence with the
316 previous reports[47]. In inherited muscle diseases, damaging variants in the disease-associated gene can
317 result in mislocalization and accumulation of mutant protein in the muscle fibers. Previous studies
318 have reported rare exonic variants in genes, including *VCP* and *SQSTM1* in IBM[48, 49]. However, in
319 our cohort of IBM patients, there were no rare exonic *TARDBP, VCP,* or *SQSTM1* variants[6] that could
320 suggest a possible association with abnormal protein turnover and accumulation/aggregation.
321 Therefore, further evidence to suggest the pathogenic role of variants in such genes and their
322 downstream effect on pathological protein accumulation in IBM is still missing. However, the
323 potential downside of TDP-43 not being available for its traditional roles, such as effective splicing,
324 because of the aggregation is noteworthy. Further evidence of possible dysregulation of splicing in
325 IBM muscles comes from our differential splicing results where proteins involved in mRNA
326 processing, transcription, and regulation are enriched, suggesting that additional studies are needed
327 to understand the possible impact of dysregulated mRNA processing in IBM muscles.

328 Previously, Pinal-Fernandez and colleagues observed that calcium-induced T lymphocyte apoptosis
329 was a significant IBM-specific dysregulated pathway in their extensive analysis of different
330 inflammatory myopathies but did not comment further on the possible importance[17]. Additionally,
331 using a smaller sample size, Amici and colleagues identified calcium signaling as one of the
332 significant disturbed pathways in IBM muscles and hypothesized its potential major role[14].
333 Furthermore, previous gene expression studies in IBM have analyzed data primarily from

microarrays[11, 12, 15]. Only recently paired-end reads RNA-seq have been used in IBM studies[13, 14, 16, 17]. While microarray-based analyses are comparable for differential expression studies, RNA-seq based methodologies are superior for in-depth transcriptome analysis. In our study design, we used matched muscle biopsies and state-of-the-art RNA-seq analysis tools. Our analyses show novel molecular events in IBM muscles which increase our understanding of IBM and provide valuable additions to improve the therapeutic interventions considering the disturbed calcium homeostasis, dysregulation of LCK, and associated deregulation of apoptotic control of T cells in IBM muscles.

Acknowledgments

The authors would like to thank the patients and their families. We thank the Oxford Genomics Centre at the Wellcome Centre for Human Genetics (funded by Wellcome Trust grant reference 203141/Z/16/Z) for the generation and initial processing of the sequencing data. We would like to thank CSC – IT Center for Science, Finland, for its computational resources. We thank Merja Soininen, Talha Qureshi and Eini Penkkimäki for their technical assistance. We would like to thank Peter-Bram 't Hoen for his critical review of this manuscript.

Funding

This work was supported by the Folkhälsan Research Foundation, Doctoral program in Integrative Life Science (ILS) and Doctoral school in Health Sciences (DSHealth), University of Helsinki (MJ), the Päivikki and Sakari Sohlberg Foundation (MJ), the Biomedicum Helsinki Foundation (MJ), Finska läkaresällskapet (BU/MJ), the Finnish Medical Foundation (JP), the Paulo foundation (MS), the Jane and Aatos Erkko Foundation (PH) and the Sigrid Jusélius Foundation (BU).

Author Contributions

MJ: Conceptualization of the study, funding acquisition, data analysis and curation, methodology, project administration, visualization, writing the original draft, review, and editing of the manuscript.

AV: data analysis, methodology, writing the original draft.

JP: Patient samples and data collection, writing the original draft.

MJ: Patient samples and data collection, review, and editing of the manuscript.

PH.J.: Conceptualization of the methodology, review, and editing of the manuscript.

JS: Data analysis, review, and editing of the manuscript.

SH: Patient samples and data collection, review, and editing of the manuscript.

MS: Conceptualization of the study and methodology, review and editing of the manuscript.

PH: Funding acquisition, project administration, and review and editing of the manuscript.

BU.: Conceptualization of the study, funding acquisition, supervision, project administration, review, and editing of the manuscript.

Conflicts of interest

The authors report no conflicts of interest.

References

1. Ikenaga C, Kubota A, Kadoya M, et al. Clinicopathologic features of myositis patients with CD8-MHC-1 complex pathology. Neurology 2017;89:1060-1068.
2. Hanna MG, Badrising UA, Benveniste O, et al. Safety and efficacy of intravenous bimagrumab in inclusion body myositis (RESILIENT): a randomised, double-blind, placebo-controlled phase 2b trial. Lancet Neurol 2019;18:834-844.
3. Cai H, Yabe I, Sato K, et al. Clinical, pathological, and genetic mutation analysis of sporadic inclusion body myositis in Japanese people. J Neurol 2012;259:1913-1922.
4. Amato AA, Shebert RT. Inclusion body myositis in twins. Neurology 1998;51:598-600.
5. Askanas V, Engel WK. Sporadic inclusion-body myositis: a proposed key pathogenetic role of the abnormalities of the ubiquitin-proteasome system, and protein misfolding and aggregation. Acta Myol 2005;24:17-24.
6. Johari M, Arumilli M, Palmio J, et al. Association study reveals novel risk loci for sporadic inclusion body myositis. Eur J Neurol 2017;24:572-577.
7. Rothwell S, Chinoy H, Lamb JA, et al. Focused HLA analysis in Caucasians with myositis identifies significant associations with autoantibody subgroups. Annals of the Rheumatic Diseases 2019;78:996-1002.
8. Askanas V, Engel WK. Sporadic inclusion-body myositis and hereditary inclusion-body myopathies: current concepts of diagnosis and pathogenesis. Curr Opin Rheumatol 1998;10:530-542.
9. Greenberg SA. Theories of the pathogenesis of inclusion body myositis. Curr Rheumatol Rep 2010;12:221-228.
10. Hiniker A, Daniels BH, Margeta M. T-Cell-Mediated Inflammatory Myopathies in HIV-Positive Individuals: A Histologic Study of 19 Cases. J Neuropathol Exp Neurol 2016;75:239-245.
11. Greenberg SA, Sanoudou D, Haslett JN, et al. Molecular profiles of inflammatory myopathies. Neurology 2002;59:1170-1182.
12. Eisenberg I, Eran A, Nishino I, et al. Distinctive patterns of microRNA expression in primary muscular disorders. Proc Natl Acad Sci U S A 2007;104:17016-17021.
13. Hamann PD, Roux BT, Heward JA, et al. Transcriptional profiling identifies differential expression of long non-coding RNAs in Jo-1 associated and inclusion body myositis. Sci Rep 2017;7:8024.
14. Amici DR, Pinal-Fernandez I, Mazala DA, et al. Calcium dysregulation, functional calpainopathy, and endoplasmic reticulum stress in sporadic inclusion body myositis. Acta Neuropathol Commun 2017;5:24.
15. Greenberg SA, Pinkus JL, Kong SW, Baecher-Allan C, Amato AA, Dorfman DM. Highly differentiated cytotoxic T cells in inclusion body myositis. Brain 2019;142:2590-2604.
16. Pinal-Fernandez I, Casal-Dominguez M, Derfoul A, et al. Identification of distinctive interferon gene signatures in different types of myositis. Neurology 2019;93:e1193-e1204.
17. Pinal-Fernandez I, Casal-Dominguez M, Derfoul A, et al. Machine learning algorithms reveal unique gene expression profiles in muscle biopsies from patients with different types of myositis. Ann Rheum Dis 2020;79:1234-1242.
18. Rose MR, Group EIW. 188th ENMC International Workshop: Inclusion Body Myositis, 2-4 December 2011, Naarden, The Netherlands. Neuromuscul Disord 2013;23:1044-1055.
19. Hackman P, Vihola A, Haravuori H, et al. Tibial muscular dystrophy is a titinopathy caused by mutations in TTN, the gene encoding the giant skeletal-muscle protein titin. Am J Hum Genet 2002;71:492-500.

416 20. Huovinen S, Penttila S, Somervuo P, et al. Differential isoform expression and selective
417 muscle involvement in muscular dystrophies. Am J Pathol 2015;185:2833-2842.
418 21. Chen S, Zhou Y, Chen Y, Gu J. fastp: an ultra-fast all-in-one FASTQ preprocessor.
419 Bioinformatics 2018;34:i884-i890.
420 22. Dobin A, Davis CA, Schlesinger F, et al. STAR: ultrafast universal RNA-seq aligner.
421 Bioinformatics 2013;29:15-21.
422 23. Liao Y, Smyth GK, Shi W. featureCounts: an efficient general purpose program for
423 assigning sequence reads to genomic features. Bioinformatics 2014;30:923-930.
424 24. Griffiths-Jones S. The microRNA Registry. Nucleic Acids Res 2004;32:D109-111.
425 25. Love MI, Huber W, Anders S. Moderated estimation of fold change and dispersion for
426 RNA-seq data with DESeq2. Genome Biol 2014;15:550.
427 26. Stephens M. False discovery rates: a new deal. Biostatistics 2016;18:275-294.
428 27. Hartley SW, Mullikin JC. QoRTs: a comprehensive toolset for quality control and data
429 processing of RNA-Seq experiments. BMC Bioinformatics 2015;16:224.
430 28. Hartley SW, Mullikin JC. Detection and visualization of differential splicing in RNA-Seq
431 data with JunctionSeq. Nucleic Acids Res 2016;44:e127.
432 29. Yu G, Wang LG, Han Y, He QY. clusterProfiler: an R package for comparing biological
433 themes among gene clusters. OMICS 2012;16:284-287.
434 30. Lex A, Gehlenborg N, Strobelt H, Vuillemot R, Pfister H. UpSet: Visualization of
435 Intersecting Sets. IEEE Transactions on Visualization and Computer Graphics 2014;20:1983-1992.
436 31. Güttsches A-K, Brady S, Krause K, et al. Proteomics of rimmed vacuoles define new risk
437 allele in inclusion body myositis. Annals of neurology 2017;81:227-239.
438 32. Joseph N, Reicher B, Barda-Saad M. The calcium feedback loop and T cell activation:
439 how cytoskeleton networks control intracellular calcium flux. Biochim Biophys Acta 2014;1838:557-
440 568.
441 33. Lewis RS. Calcium signaling mechanisms in T lymphocytes. Annu Rev Immunol
442 2001;19:497-521.
443 34. Qu B, Al-Ansary D, Kummerow C, Hoth M, Schwarz EC. ORAI-mediated calcium influx
444 in T cell proliferation, apoptosis and tolerance. Cell Calcium 2011;50:261-269.
445 35. Crabtree GR, Olson EN. NFAT signaling: choreographing the social lives of cells. Cell
446 2002;109 Suppl:S67-79.
447 36. Calnan BJ, Szychowski S, Chan FK, Cado D, Winoto A. A role for the orphan steroid
448 receptor Nur77 in apoptosis accompanying antigen-induced negative selection. Immunity
449 1995;3:273-282.
450 37. Thompson J, Winoto A. During negative selection, Nur77 family proteins translocate
451 to mitochondria where they associate with Bcl-2 and expose its proapoptotic BH3 domain. J Exp
452 Med 2008;205:1029-1036.
453 38. Liebmann M, Hucke S, Koch K, et al. Nur77 serves as a molecular brake of the
454 metabolic switch during T cell activation to restrict autoimmunity. Proceedings of the National
455 Academy of Sciences 2018;115:E8017-E8026.
456 39. Youn HD, Chatila TA, Liu JO. Integration of calcineurin and MEF2 signals by the
457 coactivator p300 during T-cell apoptosis. The EMBO journal 2000;19:4323-4331.
458 40. Youn HD, Liu JO. Cabin1 represses MEF2-dependent Nur77 expression and T cell
459 apoptosis by controlling association of histone deacetylases and acetylases with MEF2. Immunity
460 2000;13:85-94.
461 41. Palmer E. Negative selection--clearing out the bad apples from the T-cell repertoire.
462 Nat Rev Immunol 2003;3:383-391.

463 42. Raza K, Scheel-Toellner D, Lee CY, et al. Synovial fluid leukocyte apoptosis is inhibited
464 in patients with very early rheumatoid arthritis. Arthritis Res Ther 2006;8:R120.
465 43. Nakka K, Ghigna C, Gabellini D, Dilworth FJ. Diversification of the muscle proteome
466 through alternative splicing. Skeletal Muscle 2018;8:8.
467 44. Yu X-Z, Levin SD, Madrenas J, Anasetti C. Lck Is Required for Activation-Induced T Cell
468 Death after TCR Ligation with Partial Agonists. The Journal of Immunology 2004;172:1437-1443.
469 45. McNeill L, Salmond RJ, Cooper JC, et al. The differential regulation of Lck kinase
470 phosphorylation sites by CD45 is critical for T cell receptor signaling responses. Immunity
471 2007;27:425-437.
472 46. Thompson JL, Shuttleworth TJ. A plasma membrane-targeted cytosolic domain of
473 STIM1 selectively activates ARC channels, an arachidonate-regulated store-independent Orai
474 channel. Channels (Austin) 2012;6:370-378.
475 47. Cortese A, Plagnol V, Brady S, et al. Widespread RNA metabolism impairment in
476 sporadic inclusion body myositis TDP43-proteinopathy. Neurobiol Aging 2014;35:1491-1498.
477 48. Weihl CC, Baloh RH, Lee Y, et al. Targeted sequencing and identification of genetic
478 variants in sporadic inclusion body myositis. Neuromuscul Disord 2015;25:289-296.
479 49. Gang Q, Bettencourt C, Machado PM, et al. Rare variants in SQSTM1 and VCP genes
480 and risk of sporadic inclusion body myositis. Neurobiol Aging 2016;47:218 e211-218 e219.

481

Figures and tables

Figure 1: a) Workflow and methodology used in this study. b) Principal component analysis of gene expression results showing the pairwise comparison between IBM, control TMD and control amputee populations. c) IBM-specific differentially expressed genes were determined by comparing IBM cases with amputee and TMD controls. d) Comparison between IBM specific differentially expressed genes (cyan) and IBM specific differentially spliced genes (magenta).

Figure 2: a) Top 15 differentially expressed genes specific to IBM muscles. Log_2 fold change (log2FC) of IBM versus amputees calculated by DEseq2 after shrinkage estimations. '+'/'-' sign denotes the direction of change, i.e., positive log2FC values indicate overexpressed genes in IBM muscles and negative log2FC values indicate underexpressed genes in IBM muscles. The p-value of significance and adjusted p-value using the Benjamini-Hochberg corrections and associated GO terms are shown for each gene. Genes marked with * are also observed as significantly dysregulated in Hamann et al.[13] b) Normalized gene expression in the different cohorts is presented as boxplots. Median and quartile values are shown with whiskers reaching up to 1.5 times the interquartile range. Individual expression levels are shown as jitter points. The raincloud plots illustrate the distribution of data in each cohort. The scaled Y-axis shows log normalized counts.

Figure 3: a) Top 10 dysregulated canonical pathways identified by IPA. The significance of the identified pathway is shown with a p-value and the number of differentially expressed genes observed in the IBM-specific dataset compared to the number of genes present in the database for each pathway. b) In cell signaling processes, different pathways associated with calcium homeostasis are shown along with their p-value and a prediction state. c) in the long non-coding RNA analysis, upstream binding partners are shown along with their target lncRNA. A p-value and associated GO terms are shown. d) in the miRNA analysis, upstream binding partners are shown along with their target miRNA. A p-value and associated GO terms are shown.

Figure 4: The calcium-induced T lymphocyte apoptosis pathway with gene expression changes observed in IBM compared to controls. Created with BioRender.com

Figure 5. Statistical over-representation tests were performed on a list of differentially spliced RNAs, using clusterProfiler for a) Biological Processes, b) Cellular component, and c) Molecular function. d) An UpSet plot is shown comparing six different sets, namely, IBM specific differentially spliced (1,271 genes), mobilization of Ca^{2+} (80 genes), calcium-induced T lymphocyte apoptosis (69 genes), the flux of Ca^{2+} (51 genes), quantity of Ca^{2+} (51 genes), and release of Ca^{2+} (33 genes). Dots and lines represent subsets of different lists. The horizontal bar graph (wine color) represents the size of each set, while the vertical histogram (black) represents the number of RNAs in each subset. The 10 RNAs that are both differentially expressed and differentially spliced are shown with a red circle with their gene names (black).

Figure 6. a) Normalized LCK expression in the different cohorts (as explained in Fig 2b). b) Altered isoform expression of *LCK* using JunctionSeq showing estimated normalized mean read-pair count for each exon and splice junctions in the different cohorts (left) as well as for the whole *LCK* gene (right). The significantly alternatively spliced feature, E016 (pink), corresponds to chr1:32274818-32274992 (GRCh38). The alternative *LCK* transcripts used in the JunctionSeq analysis are shown below with their corresponding ENSEMBL identifiers.

a

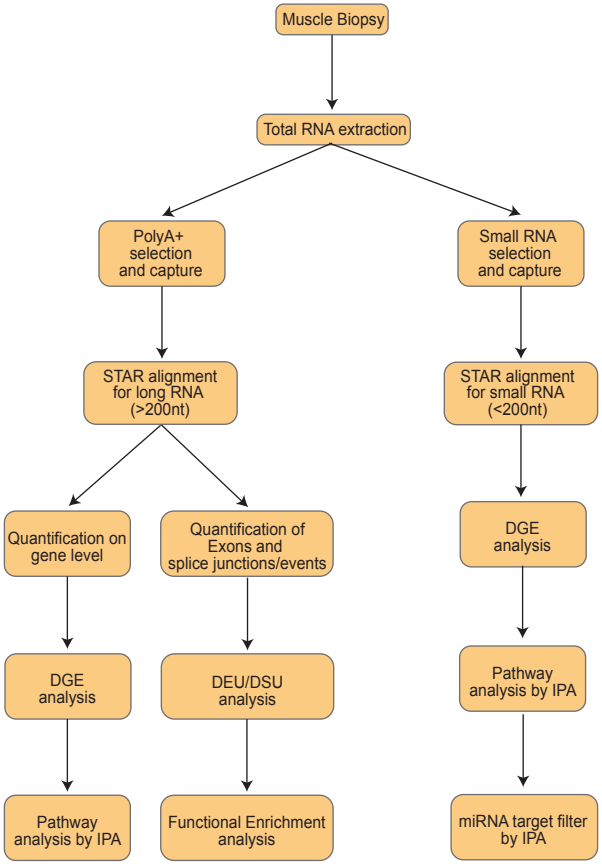
Muscle Biopsy
Total RNA extraction
PolyA+ selection and capture
Small RNA selection and capture
STAR alignment for long RNA (>200nt)
STAR alignment for small RNA (<200nt)
Quantification on gene level
Quantification of Exons and splice junctions/events
DGE analysis
DGE analysis
DEU/DSU analysis
Pathway analysis by IPA
Pathway analysis by IPA
Functional Enrichment analysis
miRNA target filter by IPA

c

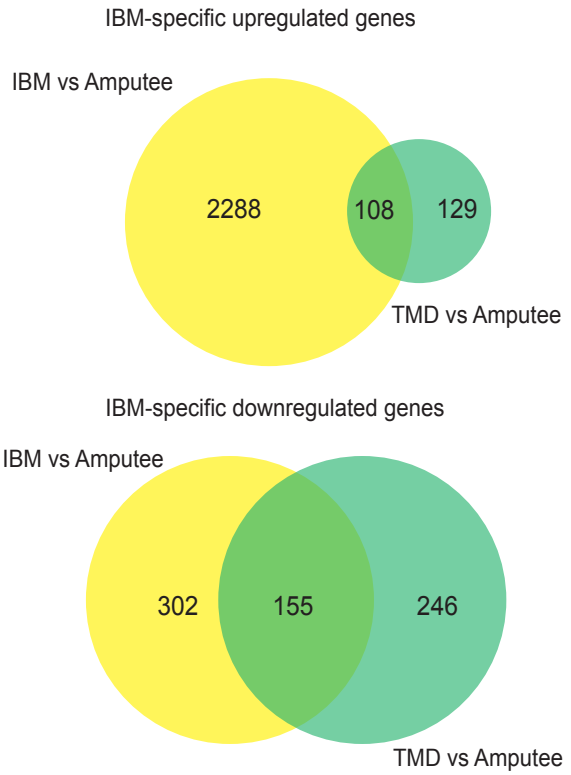
IBM-specific upregulated genes
IBM vs Amputee
2288
108
129
TMD vs Amputee
IBM-specific downregulated genes
IBM vs Amputee
302
155
246
TMD vs Amputee

b

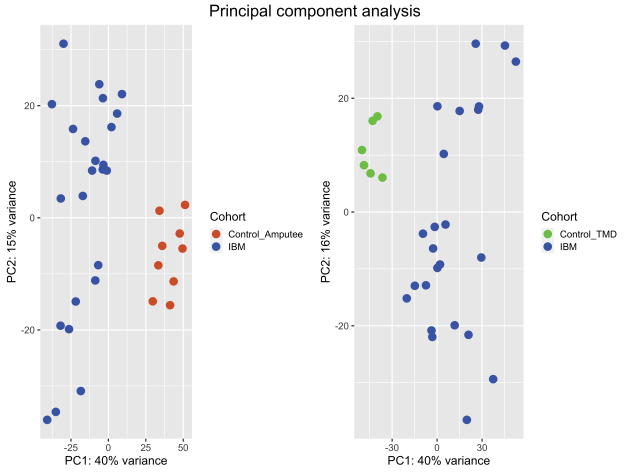
Principal component analysis
PC2: 15% variance
PC1: 40% variance
Cohort
Control_Amputee
IBM
PC2: 16% variance
PC1: 40% variance
Cohort
Control_TMD
IBM

d

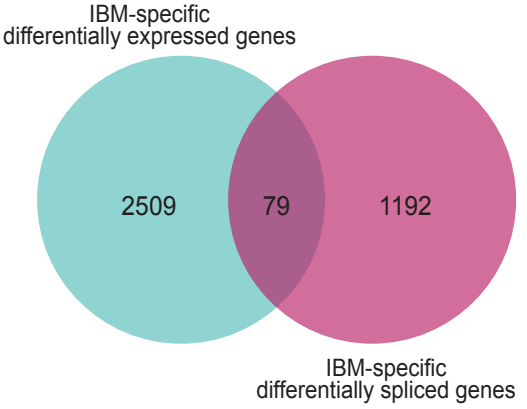
IBM-specific differentially expressed genes
2509
79
1192
IBM-specific differentially spliced genes

a

Symbol	Mean count	log2FC	pvalue	padj	GO terms
KDM7A	1147.06	-1.69	4.07E-32	2.39E-28	Iron ion binding and oxidoreductase activity
LGALS3BP*	2922.28	2.59	5.91E-31	2.89E-27	Scavenger receptor activity
TLR3	128.42	2.29	3.98E-28	1.30E-24	Regulation of dendritic cell cytokine production
ATP6V0A1	3393.79	-1.76	3.01E-27	8.83E-24	ATPase binding and proton-transporting ATPase activity
IRF8*	199.90	3.89	4.66E-27	1.24E-23	DNA-binding transcription factor activity, RNA polymerase II-specific
SLC7A7	216.91	3.16	2.08E-26	5.09E-23	Amino acid transmembrane transporter activity
FGL2	1102.10	3.27	3.14E-26	6.58E-23	T cell activation via T cell receptor contact with antigen bound to MHC molecule on antigen presenting cell
B2M*	46381.30	2.29	4.71E-26	9.22E-23	Positive regulation of T cell mediated cytotoxicity
MYL4*	610.22	5.44	5.92E-26	1.09E-22	Actin monomer binding, Calcium ion binding
UBE2L6*	986.03	2.47	1.86E-25	3.04E-22	Ubiquitin-protein transferase activity
SPPL2B	1161.90	-1.66	2.99E-25	4.39E-22	Protein homodimerization activity
TUBA1A*	2951.15	2.50	4.36E-25	5.81E-22	GTPase activity, structural molecule activity
TFAP4	234.41	-1.52	4.32E-25	5.81E-22	Transcription regulatory region sequence-specific DNA binding
HLA-DRA	8658.66	3.25	7.29E-25	9.00E-22	Antigen processing and presentation of endogenous peptide antigen via MHC class II
SOX11	96.02	4.03	1.97E-24	2.23E-21	DNA-binding transcription factor activity, RNA polymerase II-specific

b

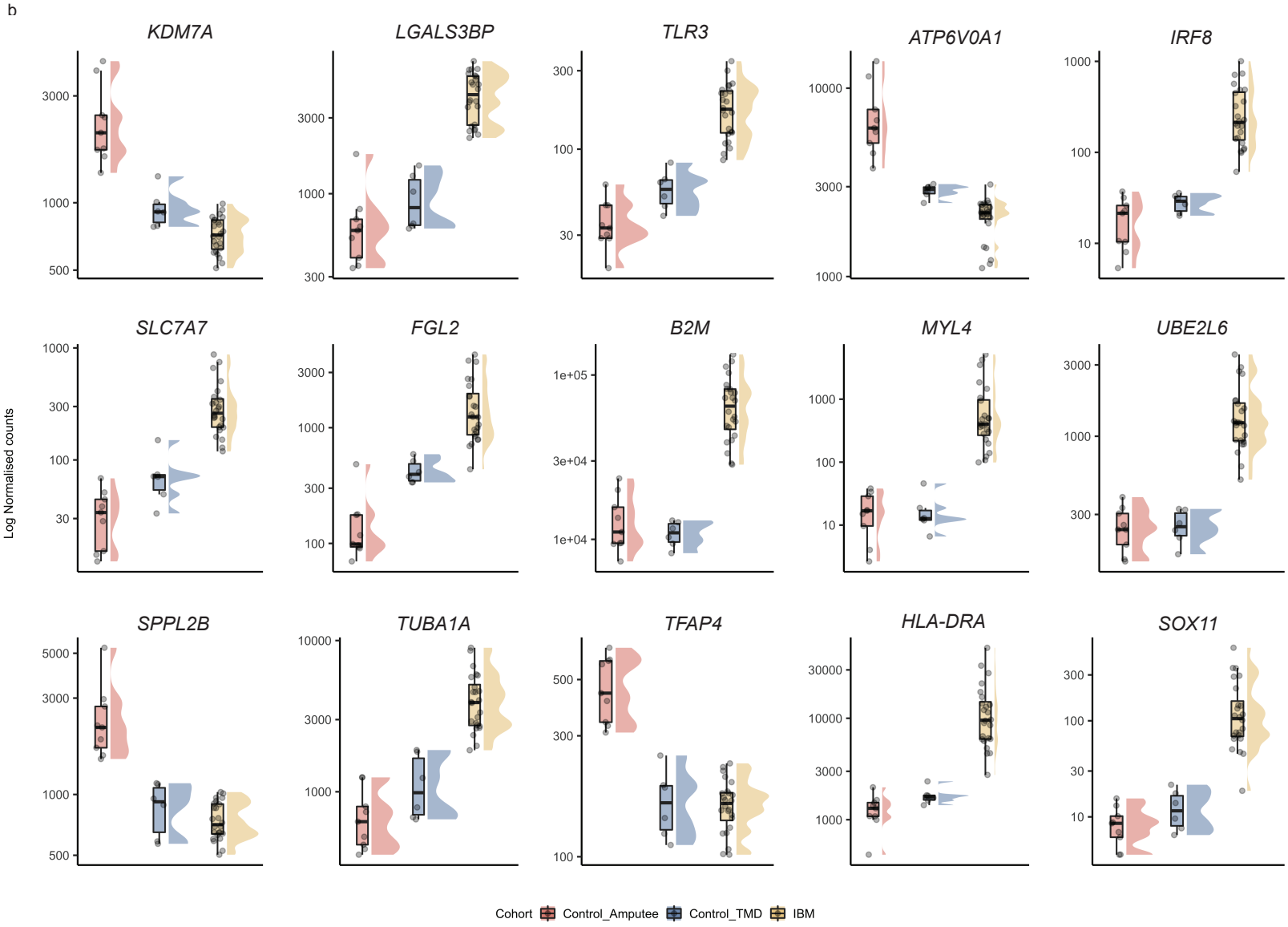

a

Ingenuity Canonical Pathways	p-value	Number of genes in dataset / Number of genes in database	z-score
Dendritic Cell Maturation	5.72E-31	106/357	7.02
T Cell Receptor Signaling	2.30E-25	97/355	8.981
T Cell Exhaustion Signaling Pathway	3.12E-25	94/338	2.191
Cdc42 Signaling	7.63E-24	88/315	3.3
iCOS-iCOSL Signaling in T Helper Cells	4.10E-23	81/280	5.099
CD28 Signaling in T Helper Cells	1.13E-22	82/290	3.578
OX40 Signaling Pathway	4.03E-21	68/222	1.633
Calcium-induced T Lymphocyte Apoptosis	1.29E-20	69/232	4.359
Nur77 Signaling in T Lymphocytes	3.07E-20	72/253	3.162
Role of NFAT in Regulation of the Immune Response	4.57E-19	87/360	5.916

b

Functional annotations	p-value	Predicted activation state
Mobilization of Ca^{2+}	5.04E-26	Increased
Flux of Ca^{2+}	4.68E-13	Increased
Quantity of Ca^{2+}	4.34E-09	Increased
Release of Ca^{2+}	5.00E-09	Increased

c

Upstream regulator	Target molecule in dataset	p-value	GO terms and annotations
JDP2	*DNM3OS*	4.10E-03	DNA-binding transcription factor activity, RNA polymerase II-specific
miR-338-3p	*NR2F1-AS1*	4.10E-03	Negative regulation of gene expression; negative regulation of IL-6 production; negative regulation of cytokine production involved in inflammatory response
miR-150-5p	*MIAT*	4.10E-03	mRNA binding involved in posttranscriptional gene silencing
TARDBP	*MIAT*	2.03E-02	RNA polymerase II cis-regulatory region sequence-specific DNA binding
mir-150	*MIAT*	2.63E-02	mRNA binding involved in posttranscriptional gene silencing
PGF	*DNM3OS*	3.43E-02	Protein binding, signal transduction
FUS	*RMRP*	3.43E-02	mRNA binding, mRNA stabilization
DDX58	*EGOT*	4.61E-02	double-stranded RNA binding

d

Upstream regulator	p-value	GO terms and annotations
AGO2	7.89E-23	RNA polymerase II complex binding
SSB	4.74E-19	RNA binding
TP53	7.59E-09	Transcription regulatory region sequence-specific DNA binding
RNA polymerase III	4.09E-06	Synthesis of small RNA, RNA polymerase activity

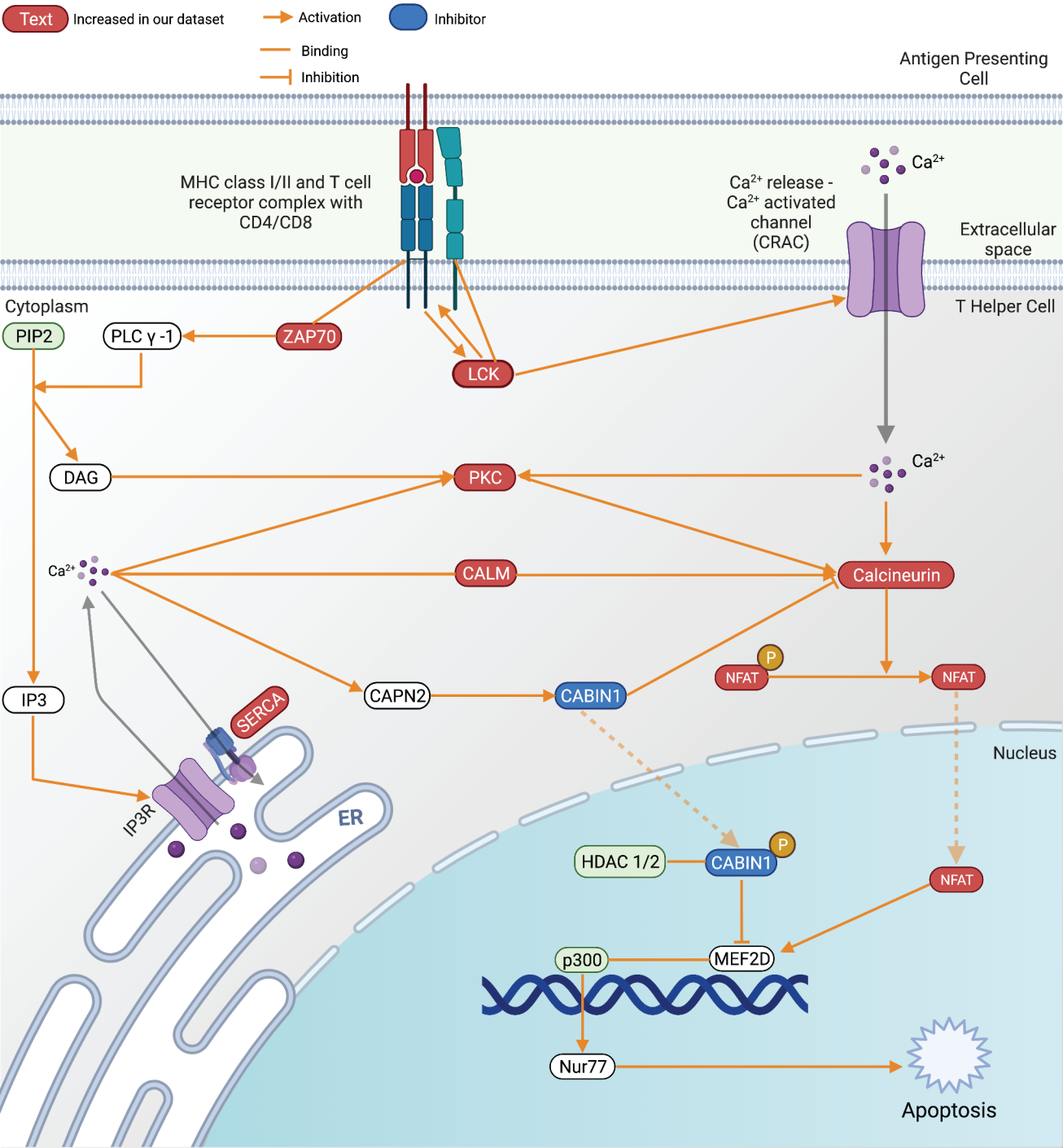
Text
Increased in our dataset
Activation
Inhibitor
Binding
Inhibition
Antigen Presenting Cell
MHC class I/II and T cell receptor complex with CD4/CD8
Ca2+ release - Ca2+ activated channel (CRAC)
Ca2+
Extracellular space
T Helper Cell
Cytoplasm
PIP2
PLC γ -1
ZAP70
LCK
DAG
PKC
Ca2+
CALM
Calcineurin
NFAT
P
NFAT
IP3
CAPN2
CABIN1
SERCA
IP3R
ER
Nucleus
HDAC 1/2
CABIN1
P
NFAT
p300
MEF2D
Nur77
Apoptosis

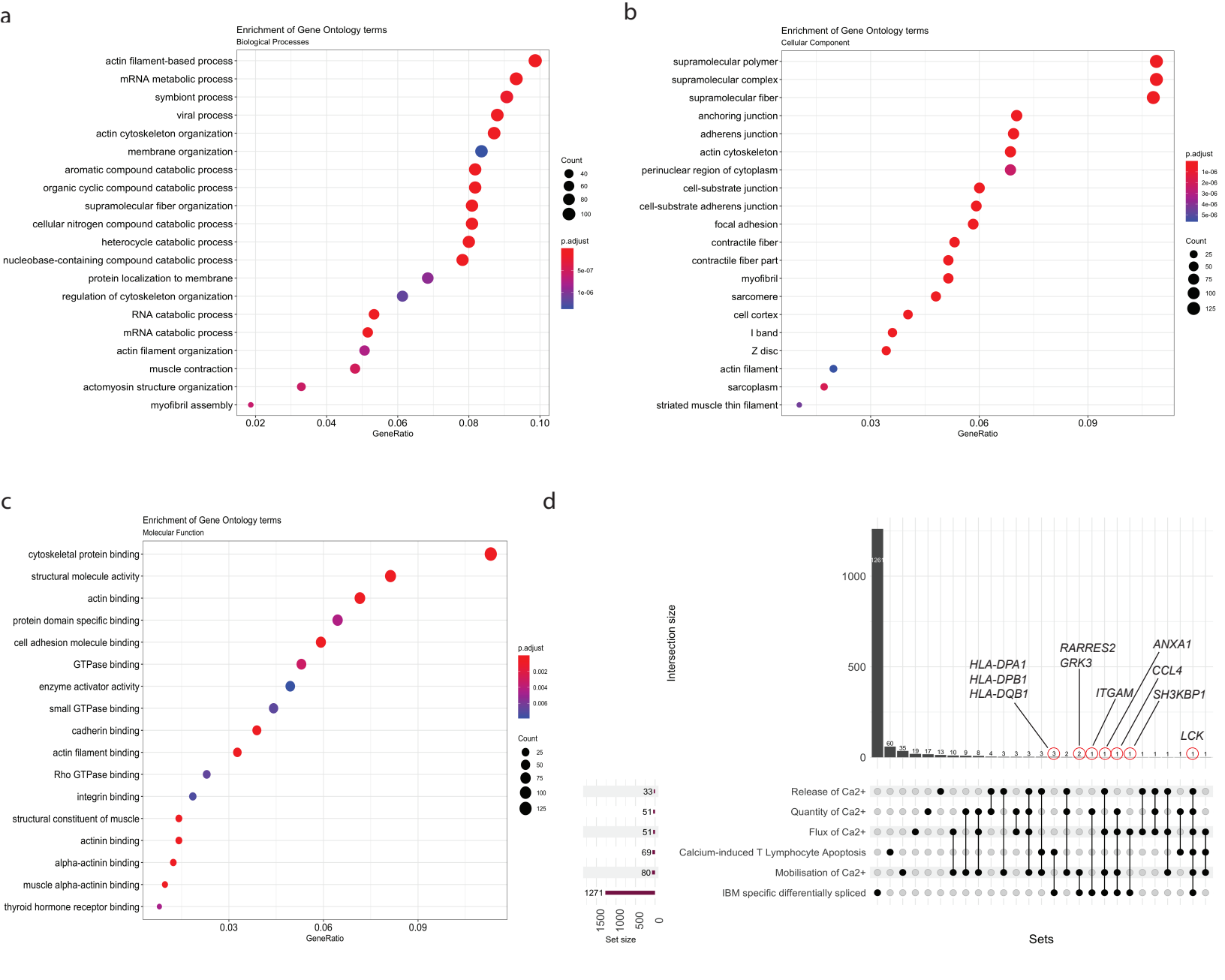
a
Enrichment of Gene Ontology terms
Biological Processes
actin filament-based process
mRNA metabolic process
symbiont process
viral process
actin cytoskeleton organization
membrane organization
aromatic compound catabolic process
organic cyclic compound catabolic process
supramolecular fiber organization
cellular nitrogen compound catabolic process
heterocycle catabolic process
nucleobase-containing compound catabolic process
protein localization to membrane
regulation of cytoskeleton organization
RNA catabolic process
mRNA catabolic process
actin filament organization
muscle contraction
actomyosin structure organization
myofibril assembly
0.02
0.04
0.06
0.08
0.10
GeneRatio
Count
40
60
80
100
p.adjust
5e-07
1e-06
b
Enrichment of Gene Ontology terms
Cellular Component
supramolecular polymer
supramolecular complex
supramolecular fiber
anchoring junction
adherens junction
actin cytoskeleton
perinuclear region of cytoplasm
cell-substrate junction
cell-substrate adherens junction
focal adhesion
contractile fiber
contractile fiber part
myofibril
sarcomere
cell cortex
I band
Z disc
actin filament
sarcoplasm
striated muscle thin filament
0.03
0.06
0.09
GeneRatio
p.adjust
1e-06
2e-06
3e-06
4e-06
5e-06
Count
25
50
75
100
125
c
Enrichment of Gene Ontology terms
Molecular Function
cytoskeletal protein binding
structural molecule activity
actin binding
protein domain specific binding
cell adhesion molecule binding
GTPase binding
enzyme activator activity
small GTPase binding
cadherin binding
actin filament binding
Rho GTPase binding
integrin binding
structural constituent of muscle
actinin binding
alpha-actinin binding
muscle alpha-actinin binding
thyroid hormone receptor binding
0.03
0.06
0.09
GeneRatio
p.adjust
0.002
0.004
0.006
Count
25
50
75
100
125
d
Intersection size
1000
500
0
1261
60
35
19
17
13
10
9
8
4
3
3
3
3
3
2
2
1
1
1
1
1
1
1
1
1
HLA-DPA1
HLA-DPB1
HLA-DQB1
RARRES2
GRK3
ITGAM
ANXA1
CCL4
SH3KBP1
LCK
Release of Ca2+
Quantity of Ca2+
Flux of Ca2+
Calcium-induced T Lymphocyte Apoptosis
Mobilisation of Ca2+
IBM specific differentially spliced
33
51
51
69
80
1271
1500
1000
500
0
Set size
Sets

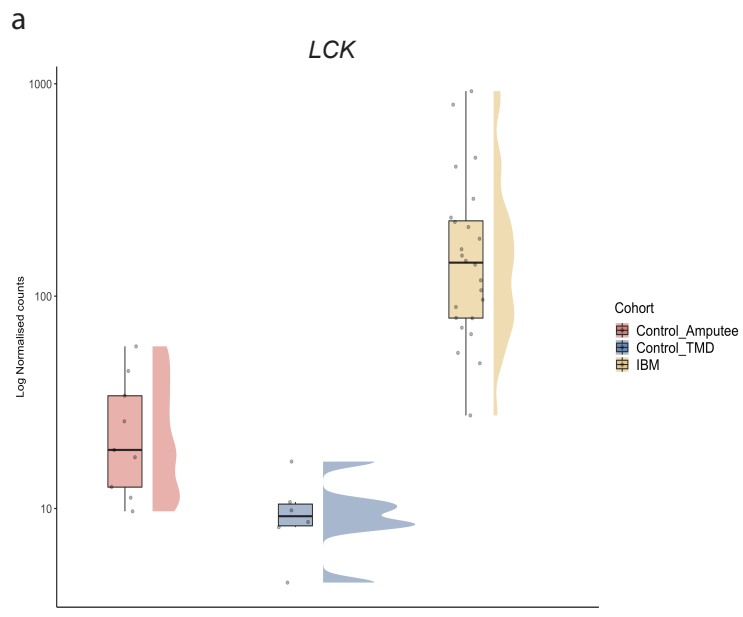
a
LCK
Log Normalised counts
1000
100
10
Cohort
Control_Amputee
Control_TMD
IBM

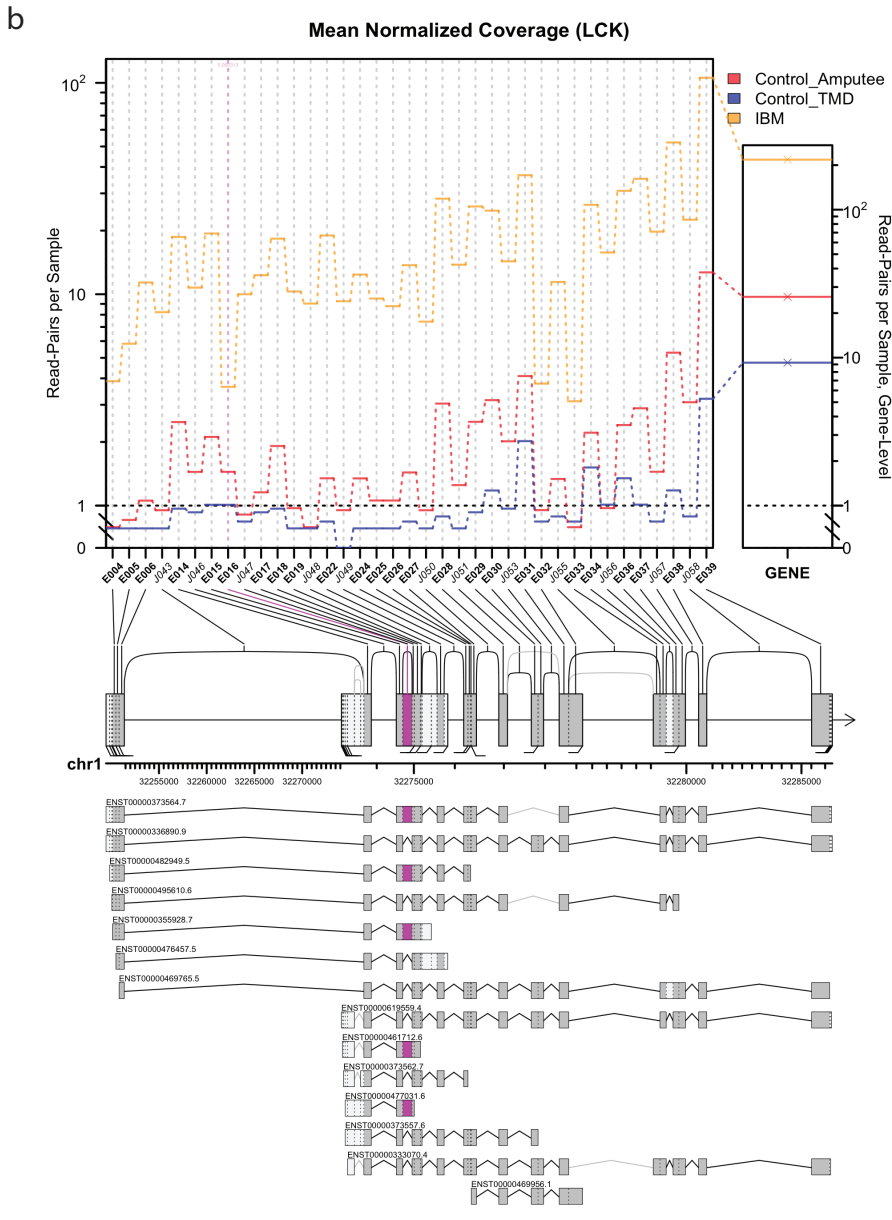
b
Mean Normalized Coverage (LCK)
Read-Pairs per Sample
Read-Pairs per Sample, Gene-Level
Control_Amputee
Control_TMD
IBM
GENE
chr1
32255000
32260000
32265000
32270000
32275000
32280000
32285000
ENST00000373564.7
ENST00000336890.9
ENST00000482949.5
ENST00000495610.6
ENST00000355928.7
ENST00000476457.5
ENST00000469765.5
ENST00000619559.4
ENST00000461712.6
ENST00000373562.7
ENST00000477031.6
ENST00000373557.6
ENST00000333070.4
ENST00000469956.1